Bonded water is an integral component of dissolved organic matter in the ocean

Kaijun Lu[1], Xiao You[2#], Laodong Guo[3], Carlos Baiz[2], Zhanfei Liu[1*]

[1]Marine Science Institute, The University of Texas at Autin, Port Aransas, Texas 78418, USA
[2]Department of Chemistry, The University of Texas at Austin, Austin, Texas 78712, USA
[3]School of Freshwater Sciences, University of Wisconsin-Milwaukee, Milwaukee, Wisconsin 53204, USA
[#]Current address: School of Engineering, Westlake University, Hangzhou, Zhejiang 310030, China
[*]Corresponding: zhanfei.liu@utexas.edu

Abstract

Dissolved organic matter (DOM) in the ocean, as one of the largest pools of reduced carbon on Earth, plays an important role in the global carbon cycle, yet its chemical structure remains largely unknown. Here we show that high molecular weight DOM (HMW-DOM) contains approximately 10% bonded water (H_2O) by weight. The bonded H_2O molecules are an integral part of the DOM organic complex, likely maintained through strong intermolecular hydrogen bonds, as the H_2O is not released during freeze drying and barely exchangeable with surrounding H_2O in solution. When the bonded H_2O was removed by mild heating (70 °C), the HMW-DOM became more bioavailable as shown by laboratory incubation experiments. These findings suggest that the bonded H_2O plays a key role in regulating the stability and biogeochemical cycling of DOM in the ocean.

Oceanic dissolved organic matter (DOM), containing 660×10^{15} g of carbon (*1*) as well as other essential elements, serves as an important reservoir of reduced carbon (C) in the global C cycle and related biogeochemical processes. Much research has been devoted to investigating the chemical composition of DOM, aiming to elucidate its sources, transformations, and sinks and thus shed light on reasons for its long-term stability in millennial timescales. However, unraveling molecular-level structure and interactions in DOM has been hindered by challenges in isolating and characterizing these organic molecules (*2*). To separate oceanic DOM (concentrations typically < 1 part per million) from inorganic sea salts (at ca. 35 part per thousand), isolation techniques based on molecular size (i.e., ultrafiltration; *3*–*6*) or physical and chemical properties (i.e., solid phase extraction; *7*–*9*) of DOM have been widely applied, although the exact molecular level information on different size-fractions, especially the un-extractable DOM, still remains elusive.

The synergistic integration of cutting-edge techniques, including high-performance separation (e.g., liquid chromatography), high-resolution spectroscopy (e.g., infrared spectroscopy, mass spectrometry, and nuclear magnetic resonance spectroscopy), and mathematical data treatment, has provided insights into chemical composition, molecular formula, as well as functional groups of DOM (*10*). Notably, the combined application of mass spectrometry (MS) and nuclear magnetic resonance (NMR) spectroscopy has confirmed the existence of structures enriched in carboxyl groups (*11*) and carotenoid degradation products (*12*) in the isolated DOM. However, the mechanisms on how these structures are assembled and to what extent these structures can represent the total refractory pool of DOM remain unclear.

An illustrative example highlighting our limited understanding of DOM structure stems from the discrepancy in DOM molecular weight obtained through ultrafiltration and MS analysis (*11*, *13*), which has not been reconciled thus far. The combination of ultrafiltration, size exclusion chromatography and flow field-flow fractionation, has identified a high molecular weight fraction (HMW, size > 1 nm, molecular weight >1 kDa) in DOM (e.g., *14*). However, subsequent high-resolution MS analysis reveals that the molecular weight of HMW-DOM after ionization is in a small range of 200 – 600 Da, with the maximum intensity at ca. 400 Da (e.g., *13*). Even though it has been proposed that the observed lower molecular weight range may be a result of ionization or preferential detection with high-resolution MS (*15*), the actual molecular weight of the "HMW-DOM" still remains unclear. Alternatively, the seemingly HMW-DOM may consist of aggregated small molecules (*13*, *16*). These interconnected DOM molecules may remain integrative during the ultrafiltration process but are disassembled during the electrospray ionization (ESI) before mass spectrometry analysis.

The concept of assembling small molecules into supramolecules has been proposed in soil science to explain the chemical structure of humic substances, which are operationally defined as the colored ubiquitous recalcitrant organic compounds naturally formed from the long-term decomposition of biomass. While the exact structural characteristics of humic substances remain a topic of debate, two main hypotheses have emerged (*17*, *18*). Early studies suggested that humic substances consist of macromolecules with molecular weight in the range of tens to hundreds of kDa, while more recent studies proposed that humic substances are, in fact, supramolecular mixtures composed of relatively small compounds held together by non-covalent interactions, such as hydrogen bonds and hydrophobic

interactions (*19–22*). Notably, H_2O molecules have been shown to be a key for the stabilization of the humic substances, as well as the maintenance of its large apparent molecular size (*20*, *23*, *24*).

The role of H_2O in shaping the higher-order structures, dynamics, and functions of biomolecules has long been recognized. For example, H_2O helps maintaining the structural integrity of carbohydrates (e.g., *25*, *26*). Interactions between carbohydrates and H_2O molecules influence the connectivity of oligosaccharides through competitive intermolecular hydrogen bonding (e.g., *27*), and are vital in forming protein-carbohydrate complexes (e.g., *28*). Given that HMW-DOM is enriched with carbohydrate-like structures (e.g., *29*, *30*), we hypothesize that a fraction of H_2O may be tightly bonded in oceanic DOM, and affects its higher-order structure and bioavailability.

To test this hypothesis, we applied thermochemical and spectroscopic techniques to determine the bonded H_2O in HMW-DOM and examined how the bonded H_2O affected its bioavailability. We discovered that there are about 10% (by weight) bonded H_2O molecules in freeze-dried HMW-DOM from aquatic environments. These molecules were tightly bonded, preventing readily exchange with ambient H_2O, resembling the phenomenon of "non-freezing" H_2O in polymers (*31–33*). Further incubation experiments indicated that these bonded H_2O molecules slightly increased the recalcitrance of DOM in seawater. Our findings underscore the crucial role of bonded H_2O in dictating intermolecular interactions within DOM and, consequently, the structural integrity of DOM molecules and their biogeochemical cycling in the ocean.

The presence of H_2O in HMW-DOM. To confirm the presence of H_2O in freeze-dried HMW-DOM, thermogravimetric analysis (TGA) and evolved gas analysis (EGA) coupled with gas chromatography mass spectrometer (GC-MS) were applied. The TGA result showed that ca. 10% of HMW-DOM (by weight) was lost at a low temperature range of 25 – 100 °C. In contrast, only 1% weight was lost for DOM isolated via solid phase extraction (SPE DOM; *30*) during the same heating process (Figure 1A). The compounds lost during this temperature range were identified by EGA GC-MS. The total ion chromatogram (TIC) of EGA (Figure 1B, black) resembled the first derivative of TGA (Figure 1A), with the maximum weight loss rate/maximum components volatilization rate at ca. 100 °C in the low temperature range. Over 88% (based on ion intensities) of the detected volatile components before 200 °C have a molecular weight of 18 Da (Figure 1B, red), whereas contributions from other molecular weights (e.g., 32 and 44) were minimal (Figure S1). Given the relatively low abundance of heavier stable isotopes, namely ^2H and ^{18}O, H_2O is the only plausible candidate for the detected peak with a molecular weight 18 Da under electron impact ionization (EI).

There are several possible explanations for the released H_2O: (1) residual from an incomplete freeze-drying process; (2) byproduct produced during the heating process (e.g., through esterification or Maillard reaction); or (3) intact molecules as part of the intrinsic structure of HMW-DOM but become volatile when the heating energy is high enough. The first possibility is rejected as the free H_2O molecules should all be sublimed during the 48-hour freeze-drying process (e.g., *34*). There was little loss in the same temperature range when using standard compounds (e.g., glucose, phenylalanine) treated with the same freeze-drying protocol (Figure S2A – C). Moreover, the incomplete freeze-drying process could not

explain why the TGA results of HWM DOM and SPE DOM differed, since both went through the same freeze-drying process.

The possibility that H_2O is produced from pyrolysis process can be ruled out from the energy perspective. The pyrolysis of complex mixtures, such as lignin and humic acid, did not show a significant weight loss in 25 – 100 °C (Figure S2D and E), indicating that the released H_2O from HMW-DOM was not newly produced by the heating. In fact, much higher temperature is needed to produce H_2O from chemical reactions. The anoxic pyrolysis of a glucose and phenylalanine mixture (1:1, w/w) hardly show any weight change until the temperature reached 170 °C (Figure S2F). Particularly, the observed high reaction temperature here is consistent with previous studies on Maillard reaction, showing a much higher temperature was required for the dehydration reaction to occur under solid and dry conditions (e.g., *35*, *36*).

The stability and chemical nature of bonded H_2O in DOM. Therefore, the released H_2O molecules were originally stabilized within the HMW-DOM matrix through strong intermolecular forces, i.e., hydrogen bonding. The presence of intact H_2O molecules was further validated through Fourier transform infrared spectroscopy (FTIR) analysis. A small band corresponding to D_2O (O-D stretching region) was observed after the HMW-DOM was dissolved in D_2O at ca. 50 °C for 8 hours and then freeze-dried (Figure 2). This result not only confirms the presence of H_2O in HMW-DOM, but also indicates a very limited yet detectable exchange between the bonded H_2O molecules in solution D_2O, showing that the molecules are tightly bound even when HMW-DOM is dissolved in solution. Protein-bonded H_2O typically exhibits fast exchange dynamics ranging from pico- to millisecond (*37*), whereas the HMW-DOM here showed a much slower and more limited exchanging behavior.

To further examine the exchange capacity of bonded H_2O molecules, an exchange experiment was conducted by dissolving HMW-DOM in D_2O at a temperature of 65 °C for an extended duration. The intensity of D_2O and H_2O from EGA was analyzed to track the exchange process with time. Within the first 24 h, the D_2O/H_2O ratio slightly increased from 0.200% to 0.204% (Figure 3), consistent with the previous FTIR results (Figure 2). However, after this initial increase, the amount of exchanged D_2O remained relatively constant throughout the rest of the experiment. The pattern of D_2O exchange can be depicted by a two-stage function, characterized by a linear increase in the amount of D_2O within the first 24 h, followed by a stable D_2O/H_2O ratio (Figure 3). The observed increase in the D_2O/H_2O ratio was rather insignificant ($p = 0.50$), and the overall small D_2O/H_2O ratio remained constant over the course of the experiment. Whether the pattern of the D_2O/H_2O changes over a longer time scale remains to be elucidated. Nonetheless, these results confirm that the H_2O molecules in HMW-DOM are tightly bonded and exhibit limited exchange with ambient H_2O.

Even though the exact nature of these bonds remains unclear, intermolecular non-covalent interactions, such as hydrogen bond (H-bond), are the most likely candidate. The bonded H_2O in the HMW-DOM was released in the temperature range of 25 – 100 °C (Figure 1A), corresponding to activation energy of ca. 75 $kJ \cdot mol^{-1}$ (*30*, *38*, *39*). This energy level falls into the category of strong or low-barrier H-bonds, which is a mixture of both partially covalent and strong electrostatic contributions, and can have energy over 100 $kJ \cdot mol^{-1}$ (*40*, *41*).

These strong H-bonds tend to form between hydroxyl and carbonyl groups (e.g., resonance-assisted H-bonds) or between charged atoms (e.g., charge-assisted H-bonds; *42*), whereas moderate or weak H-bonds are generally formed between uncharged hydroxyl and amide groups (*41*). The interactions between H_2O molecules and these functional groups can be reflected in the changes of functional groups' stretching frequencies in FTIR. For instance, the interaction of -OH in H_2O with one of the lone electron pairs of the C=O oxygen atom will increase the polarization of the electron distribution in C=O, leading to a reduced stretching frequency (i.e., red shift; *43*). This phenomenon is observed in the FTIR of HMW-DOM. Compared to SPE DOM, which has minimal bonded H_2O (Figure 1A), the carbonyl region in HMW-DOM exhibits a significant red shift from the typical frequency of ca. 1700 cm^{-1} to ca. 1620 cm^{-1} (Figure 4A&B), suggesting potential interactions with H_2O molecules. In addition, compared with original HMW-DOM, HMW-DOM with bonded-H_2O removed (thereafter as H_2O-less HMW-DOM; obtained through low temperature pyrolysis, see method section for details) indeed showed a slight blueshift in the carbonyl region (Figure S3). Moreover, two-dimensional infrared spectroscopy (2D IR), which measures a 2D map of frequency correlations in the sample, provides support to this hypothesis (*44–46*). Measured 2D IR spectra exhibit a red-shift in the carbonyl groups and coupling between the O-D/O-H vibrations and –C=O stretching vibrations (Figure S4). Furthermore, the spectra show a high degree of heterogeneity in the carbonyl frequencies, indicating that there is a broad range of microenvironments. Given that hydrogen bonding is the primary interaction that shifts the –C=O stretching frequencies, the width of the features indicates that indeed H_2O is likely hydrogen bonded, and that H-bonding leads to a range of environments. On the other hand, the interactions between H_2O molecules and -OH groups in HMW-DOM cannot be explicitly observed due to spectral overlap between the O-H stretching vibration. However, this possibility cannot be ruled out, as SPE DOM, which has little bonded H_2O, also shows a relatively low -OH abundance (Figure 4A). Such coincidence may suggest a connection between H_2O and -OH groups.

Given the relative wide C content ranging from ca. 20% to over 45% for the HMW-DOM (e.g., *30*, *47*), the observed 10% H_2O by weight equals to 1 H_2O molecule for every 4 – 6 C atoms. A hypothetical structure of a hydrated HMW-DOM molecule is proposed based on our results, with a molecular weight of 1253 Da ($C_{41}H_{79}N_3O_{40}$) including 7 H_2O (Figure 4C). The proposed structure is consistent with the element stoichiometry of HMW-DOM from NMR results (*15*, *30*, *48*, *49*). The H_2O molecules are interacting with the O in carboxyl groups, considering that almost all carbonyl O in HMW-DOM is in the form of carboxyl and/or amide groups (i.e., little ketone or aldehyde groups; *48*, *50*), and the O in hydroxyl groups.

The bonded H_2O molecules therefore may change the existing paradigm regarding the molecular weight distribution of HMW-DOM. From the proposed structure, the molecular size of single "HMW-DOM" is relatively small (averaged molecular weight of ca. 376 Da; Figure 4C), yet the aggregated molecule has an apparent size of over 1200 Da, allowing the assemblage to be retained by ultrafiltration. During the MS analysis, compounds are ionized through electrospray ionization (ESI). The desolvation process, which is known as the decrease of droplet size of analytes via heat and Coulomb fissions (*51*), may lead to the disruption of H-bonds. Such disruption is especially prominent for supramolecule formed by smaller molecules, due to the limited number of noncovalently interacting atoms (*52*). With large

aggregates or assemblages connected through H-bonds disrupted, the molecules detected by the MS will mainly be the unbonded individual ones with much smaller weight.

A recent study using diffusion-ordered spectroscopy NMR (DOSY-NMR) estimated a molecular weight of approximately 5.6 kDa for HMW-DOM collected from ocean surface water (*15*). Assuming a similar bonded H_2O content of 10%, the molecular weight of 5.6 kDa corresponds to roughly 31 H_2O molecules per HMW-DOM molecule. More studies are needed to find out the reason behind the similarity between the calculated number of H_2O molecules and the average degree of polymerization (DP) for the acylpolysaccharides (APS) fraction in marine HMW-DOM (35 sugars; *15*). Nevertheless, our results do suggest a significant role of H_2O molecules in forming the saccharide network within HMW-DOM.

The impact of bonded H_2O on bioavailability of HMW-DOM. To further examine the impact of bonded H_2O molecules on the bioavailability of HMW-DOM, an incubation experiment was conducted. Once the bonded H_2O was removed by heating, HMW-DOM did not re-constitute in solution based on particle size measurement (Figure S5). During the 60-day incubation, the decrease of DOM in both treatments followed typical first-order kinetics (Figure 5). An initial decrease in DOC was observed as early as day 1, with no statistical difference between the original HMW-DOM and H_2O-less HMW-DOM during this early stage (up to day 4; $p = 0.25$, paired t-test). However, the difference became more pronounced as the incubation progressed. By day 13, ca. 15% of the initially spiked HMW-DOM was utilized, as compared to approximately 20% in H_2O-less HMW-DOM ($p = 0.08$, paired t-test). By day 30, 21% of the H_2O-less HMW-DOM was utilized, while 16% of the original HMW-DOM was removed ($p = 0.03$, paired t-test). At the end of the incubation (60 days), ca. 80% of original HMW-DOM and 65% of H_2O-less HMW-DOM remained ($p = 1.8 \times 10^{-4}$, paired t-test; Figure 5). This pattern in DOC dynamics corresponded with observed changes in dissolved oxygen (DO) levels and microbial abundance (Figure S6). The higher consumption of DO in H_2O-less HMW-DOM incubation ($p = 0.04$; paired t-test; Figure S6A) aligned with its higher microbial abundance (Figure S6B) as well as the lower concentration of DOC.

Given that the incubations of HMW-DOM and H_2O-less HMW-DOM were conducted under the same condition, the observed higher bioavailability of the latter therefore can be attributed to the loss of bonded H_2O. The 2D IR results indicated that H_2O molecules are primarily bound to the carboxyl groups in HMW-DOM, thus we hypothesize that the removal of bonded H_2O may have exposed the "protected" interior groups, making them more available to microorganisms. This idea is analogous to the enhanced decomposition activity observed in soil and sedimentary organic matter following drying and rewetting (e.g., *53–55*). However, this hypothesis needs to be validated with detailed structural information on how the loss of bonded H_2O alters the three-dimensional configuration of HMW-DOM.

Even though this work may be limited by the number of sampling locations, the samples should be representative, as HMW-DOM from different locations generally shares remarkably similar properties (e.g., *48*, *56–58*). We showed that the bonded H_2O represents 10% of HMW-DOM by weight, and these H_2O molecules were intermolecularly bonded to DOM molecules through strong H-bonds, with an energy level of ca. 75 $kJ \cdot mol^{-1}$, causing the connected DOM assemblages to be retained by ultrafiltration. As SPE DOM barely had any bonded H_2O, the weight percentage of bonded H_2O molecules in total DOM

molecules is ca. 3%, assuming HMW-DOM represents ca. 30% of total DOM in oceanic waters (*59*). These findings shed new light on a longstanding question concerning the size and structure of HMW-DOM: rather than single large molecules, the observed "large" size of HMW-DOM in natural waters can be partially attributed to smaller organic molecules forming assemblages or aggregation (> 1 kDa) through bonded H_2O. This study also revealed that the bonded H_2O influenced the bioavailability of DOM. With H_2O stabilizing the supramolecular structure of DOM, the removal of H_2O may change the conformation of HMW-DOM and expose the otherwise inaccessible moieties to microorganisms, leading to the observed faster decomposition. This work emphasizes the important role of bonded H_2O in controlling the structure of DOM and its biogeochemical cycling in the ocean, a new research avenue that needs to be further explored.

Acknowledgements

We thank the crew of R/V Pelican and Jack Lloyd for their assistance during sample collection from the Gulf of Mexico. We also thank Dr. Jian Sheng for his help with the DLS analysis. This work was funded by the Texas Sea Grant (#M1801875) and National Science Foundation (OCE #1763167 to Z.L.). L.G. acknowledges partial support from FCW (SL3.27) and NSF (#2204145).

References

1. D. A. Hansell, Recalcitrant Dissolved Organic Carbon Fractions. *Annu. Rev. Mar. Sci.* **5**, 421–445 (2013).

2. E. C. Minor, M. M. Swenson, B. M. Mattson, A. R. Oyler, Structural characterization of dissolved organic matter: a review of current techniques for isolation and analysis. *Environ. Sci. Process. Impacts* **16**, 2064–2079 (2014).

3. N. Ogura, Molecular weight fractionation of dissolved organic matter in coastal seawater by ultrafiltration. *Mar. Biol.* **24**, 305–312 (1974).

4. D. J. Carlson, M. L. Brann, T. H. Mague, L. M. Mayer, Molecular weight distribution of dissolved organic materials in seawater determined by ultrafiltration: a re-examination. *Mar. Chem.* **16**, 155–171 (1985).

5. R. Benner, "Ultra-filtration for the concentration of bacteria, viruses, and dissolved organic matter" in *Marine Particles: Analysis and Characterization* (American Geophysical Union (AGU), 1991; https://onlinelibrary.wiley.com/doi/abs/10.1029/GM063p0181), pp. 181–185.

6. L. Guo, C. H. Coleman, P. H. Santschi, The distribution of colloidal and dissolved organic carbon in the Gulf of Mexico. *Mar. Chem.* **45**, 105–119 (1994).

7. T. Dittmar, B. Koch, N. Hertkorn, G. Kattner, A simple and efficient method for the solid-phase extraction of dissolved organic matter (SPE-DOM) from seawater. *Limnol Ocean. Methods* **6**, 230–235 (2008).

8. C. Miranda, R. M. Boiteau, A. M. McKenna, A. N. Knapp, Quantitative and qualitative comparison of marine dissolved organic nitrogen recovery using solid phase extraction. *Limnol. Oceanogr. Methods* **n/a** (2023).

9. E. Jerusalén-Lleó, M. Nieto-Cid, I. Fuentes-Santos, T. Dittmar, X. A. Álvarez-Salgado, Solid phase extraction of ocean dissolved organic matter with PPL cartridges: efficiency and selectivity. *Front. Mar. Sci.* **10** (2023).

10. N. Hertkorn, C. Ruecker, M. Meringer, R. Gugisch, M. Frommberger, E. M. Perdue, M. Witt, P. Schmitt-Kopplin, High-precision frequency measurements: indispensable tools at the core of the molecular-level analysis of complex systems. *Anal. Bioanal. Chem.* **389**, 1311–1327 (2007).

11. N. Hertkorn, R. Benner, M. Frommberger, P. Schmitt-Kopplin, M. Witt, K. Kaiser, A. Kettrup, J. I. Hedges, Characterization of a major refractory component of marine dissolved organic matter. *Geochim. Cosmochim. Acta* **70**, 2990–3010 (2006).

12. N. Arakawa, L. I. Aluwihare, A. J. Simpson, R. Soong, B. M. Stephens, D. Lane-Coplen, Carotenoids are the likely precursor of a significant fraction of marine dissolved organic matter. *Sci. Adv.* **3**, e1602976 (2017).

13. T. Dittmar, A. Stubbins, Dissolved Organic Matter In Aquatic Systems. *Treatise Geochem. Second Ed. Elsevier*, 125–156 (2014).

14. Z. Zhou, B. Stolpe, L. Guo, A. M. Shiller, Colloidal size spectra, composition and estuarine mixing behavior of DOM in river and estuarine waters of the northern Gulf of Mexico. *Geochim. Cosmochim. Acta* **181**, 1–17 (2016).

15. B. N. Granzow, D. J. Repeta, What Is the Molecular Weight of "High" Molecular Weight Dissolved Organic Matter? *Environ. Sci. Technol.* **58**, 14709–14717 (2024).

16. P. Verdugo, A. L. Alldredge, F. Azam, D. L. Kirchman, U. Passow, P. H. Santschi, The oceanic gel phase: a bridge in the DOM–POM continuum. *Mar. Chem.* **92**, 67–85 (2004).

17. R. Baigorri, M. Fuentes, G. González-Gaitano, J. M. García-Mina, Simultaneous Presence of Diverse Molecular Patterns in Humic Substances in Solution. *J. Phys. Chem. B* **111**, 10577–10582 (2007).

18. R. Angelico, C. Colombo, E. Di Iorio, M. Brtnický, J. Fojt, P. Conte, Humic Substances: From Supramolecular Aggregation to Fractal Conformation—Is There Time for a New Paradigm? *Appl. Sci.* **13**, 2236 (2023).

19. A. Piccolo, The supramolecular structure of humic substances. *Soil Sci.* **166**, 810–832 (2001).

20. A. J. A. Aquino, D. Tunega, H. Pašalić, G. E. Schaumann, G. Haberhauer, M. H. Gerzabek, H. Lischka, Molecular Dynamics Simulations of Water Molecule-Bridges in Polar Domains of Humic Acids. *Environ. Sci. Technol.* **45**, 8411–8419 (2011).

21. R. Sutton, G. Sposito, M. S. Diallo, H.-R. Schulten, Molecular simulation of a model of dissolved organic matter. *Environ. Toxicol. Chem.* **24**, 1902–1911 (2005).

22. M. Orsi, Molecular dynamics simulation of humic substances. *Chem. Biol. Technol. Agric.* **1**, 10 (2014).

23. A. J. A. Aquino, D. Tunega, H. Pašalić, G. E. Schaumann, G. Haberhauer, M. H. Gerzabek, H. Lischka, Study of solvent effect on the stability of water bridge-linked carboxyl groups in humic acid models. *Geoderma* **169**, 20–26 (2011).

24. A. J. A. Aquino, D. Tunega, G. E. Schaumann, G. Haberhauer, M. H. Gerzabek, H. Lischka, Stabilizing Capacity of Water Bridges in Nanopore Segments of Humic Substances: A Theoretical Investigation. *J. Phys. Chem. C* **113**, 16468–16475 (2009).

25. J. L. Dashnau, K. A. Sharp, J. M. Vanderkooi, Carbohydrate Intramolecular Hydrogen Bonding Cooperativity and Its Effect on Water Structure. *J. Phys. Chem. B* **109**, 24152–24159 (2005).

26. J. Behler, D. W. Price, M. G. B. Drew, Water structuring properties of carbohydrates , molecular dynamics studies on 1,5-anhydro-D-fructose. *Phys. Chem. Chem. Phys.* **3**, 588–601 (2001).

27. K. N. Kirschner, R. J. Woods, Solvent interactions determine carbohydrate conformation. *Proc. Natl. Acad. Sci.* **98**, 10541–10545 (2001).

28. M. Jana, S. Bandyopadhyay, Restricted dynamics of water around a protein–carbohydrate complex: Computer simulation studies. *J. Chem. Phys.* **137**, 055102 (2012).

29. D. J. Repeta, T. M. Quan, L. I. Aluwihare, A. Accardi, Chemical characterization of high molecular weight dissolved organic matter in fresh and marine waters. *Geochim. Cosmochim. Acta* **66**, 955–962 (2002).

30. K. Lu, J. Xue, L. Guo, Z. Liu, The bio- and thermal lability of dissolved organic matter as revealed by high-resolution mass spectrometry and thermal chemical analyses. *Mar. Chem.* **250**, 104184 (2023).

31. J. Wolfe, G. Bryant, K. L. Koster, What is "unfreezable water", how unfreezable is it and how much is there? *Cryoletters* **23**, 157–166 (2002).

32. S. Li, L. C. Dickinson, P. Chinachoti, Mobility of "Unfreezable" and "Freezable" Water in Waxy Corn Starch by 2H and 1H NMR. *J. Agric. Food Chem.* **46**, 62–71 (1998).

33. V. Kocherbitov, The nature of nonfreezing water in carbohydrate polymers. *Carbohydr. Polym.* **150**, 353–358 (2016).

34. J. C. May, R. M. Wheeler, E. Grim, The determination of residual moisture in several freeze-dried vaccines and a Honey Bee Venom Allergenic Extract by TG/MS. *J. Therm. Anal.* **31**, 643–651 (1986).

35. C. W. Wong, H. B. Wijayanti, B. R. Bhandari, "Maillard Reaction in Limited Moisture and Low Water Activity Environment" in *Water Stress in Biological, Chemical, Pharmaceutical and Food Systems*, G. F. Gutiérrez-López, L. Alamilla-Beltrán, M. del Pilar Buera, J. Welti-Chanes, E. Parada-Arias, G. V. Barbosa-Cánovas, Eds. (Springer, New York, NY, 2015; https://doi.org/10.1007/978-1-4939-2578-0_4), pp. 41–63.

36. Z. Qiu, J. G. Stowell, W. Cao, K. R. Morris, S. R. Byrn, M. T. Carvajal, Effect of Milling and Compression on the Solid-State Maillard Reaction. *J. Pharm. Sci.* **94**, 2568–2580 (2005).

37. M.-C. Bellissent-Funel, A. Hassanali, M. Havenith, R. Henchman, P. Pohl, F. Sterpone, D. van der Spoel, Y. Xu, A. E. Garcia, Water Determines the Structure and Dynamics of Proteins. *Chem. Rev.* **116**, 7673–7697 (2016).

38. J. D. Hemingway, D. H. Rothman, S. Z. Rosengard, V. V. Galy, An inverse method to relate organic carbon reactivity to isotope composition from serial oxidation. *Copernic. Publ.* **14**, 5099–5114 (2017).

39. J. D. Hemingway, D. H. Rothman, K. E. Grant, S. Z. Rosengard, T. I. Eglinton, L. A. Derry, V. V. Galy, Mineral protection regulates long-term global preservation of natural organic carbon. *Nature* **570**, 228 (2019).

40. W. W. Cleland, M. M. Kreevoy, Low-Barrier Hydrogen Bonds and Enzymic Catalysis. *Science* **264**, 1887–1890 (1994).

41. G. Buemi, "Intramolecular hydrogen bonds. Methodologies and strategies for their strength evaluation" in *Hydrogen Bonding—New Insights* (Springer, 2006), pp. 51–107.

42. G. Gilli, P. Gilli, Towards an unified hydrogen-bond theory. *J. Mol. Struct.* **552**, 1–15 (2000).

43. L. Paoloni, A. Patti, F. Mangano, The hydrogen bond with carbonyl groups: theoretical study of the correlation between the X-H stretching frequency shift and the C□O group proper. *J. Mol. Struct.* **27**, 123–137 (1975).

44. P. Hamm, M. Zanni, *Concepts and Methods of 2D Infrared Spectroscopy* (Cambridge University Press, Cambridge, 2011; https://www.cambridge.org/core/books/concepts-and-methods-of-2d-infrared-spectroscopy/8D35AA43C878AF1812CDCAF8890C9FE6).

45. X. You, C. R. Baiz, Importance of Hydrogen Bonding in Crowded Environments: A Physical Chemistry Perspective. *J. Phys. Chem. A* **126**, 5881–5889 (2022).

46. M. D. Fayer, Dynamics of Liquids, Molecules, and Proteins Measured with Ultrafast 2D IR Vibrational Echo Chemical Exchange Spectroscopy. *Annu. Rev. Phys. Chem.* **60**, 21–38 (2009).

47. A. Watanabe, K. Tsutsuki, Y. Inoue, N. Maie, L. Melling, R. Jaffe, Composition of dissolved organic nitrogen in rivers associated with wetlands. *Sci. Total Environ.* **493**, 220–228 (2014).

48. D. Repeta, L. Aluwihare, "Chemical characterization and cycling of dissolved organic matter" in *Biogeochemistry of Marine Dissolved Organic Matter (Third Edition)*, D. A. Hansell, C. A. Carlson, Eds. (Academic Press, 2024; https://www.sciencedirect.com/science/article/pii/B9780443138584000113), pp. 13–67.

49. R. Benner, J. D. Pakulski, M. McCarthy, J. I. Hedges, P. G. Hatcher, Bulk chemical characteristics of dissolved organic matter in the ocean. *Science* (1992).

50. K. Whitehead, "Marine organic geochemistry" in *Chemical Oceanography and the Marine Carbon Cycle* (Cambridge University Press, 2008), pp. 261–302.

51. P. Kebarle, A brief overview of the present status of the mechanisms involved in electrospray mass spectrometry. *J. Mass Spectrom.* **35**, 804–817 (2000).

52. M. Przybylski, M. O. Glocker, Electrospray Mass Spectrometry of Biomacromolecular Complexes with Noncovalent Interactions—New Analytical Perspectives for Supramolecular Chemistry and Molecular Recognition Processes. *Angew. Chem. Int. Ed. Engl.* **35**, 806–826 (1996).

53. Z. Liu, C. Lee, Drying effects on sorption capacity of coastal sediment: The importance of architecture and polarity of organic matter. *Geochim. Cosmochim. Acta* **70**, 3313–3324 (2006).

54. Z. Liu, C. Lee, R. C. Aller, Drying effects on decomposition of salt marsh sediment and on lysine sorption. *J. Mar. Res.* **66**, 665–689 (2008).

55. Z. Liu, C. Lee, The role of organic matter in the sorption capacity of marine sediments. *Mar. Chem.* **105**, 240–257 (2007).

56. K. Lu, X. Li, H. Chen, Z. Liu, Constraints on isomers of dissolved organic matter in aquatic environments: Insights from ion mobility mass spectrometry. *Geochim. Cosmochim. Acta*, doi: 10.1016/j.gca.2021.05.007 (2021).

57. K. Lu, Z. Liu, Molecular level analysis reveals changes in chemical composition of dissolved organic matter from south Texas rivers after high flow events. *Front. Mar. Sci.* **6** (2019).

58. K. Lu, W. S. Gardner, Z. Liu, Molecular structure characterization of riverine and coastal dissolved organic matter with ion mobility quadrupole time-of-flight LCMS (IM Q-TOF LCMS). *Environ. Sci. Technol.* **52**, 7182–7191 (2018).

59. L. Guo, P. H. Santschi, A critical evaluation of the cross-flow ultrafiltration technique for sampling colloidal organic carbon in seawater. *Mar. Chem.* **55**, 113–127 (1996).

Figures

Figure 1. (A) Weight loss pattern of HMW-DOM and SPE DOM from TGA; and (B) Chromatograms of volatile component from the EGA of HMW-DOM. Shaded area in (B) indicates the region where most H_2O is detected.

Figure 2. FT-IR spectra of (A) high molecular weight DOM (HMW-DOM) obtained via ultrafiltration (red) and D_2O-exchanged HMW-DOM (blue), with the O-D stretching absorption peaks highlighted; (B) spectra of the solvent D_2O (green) and H_2O (orange) for comparison.

Figure 3. Change of D_2O/H_2O ratio during the D_2O exchange experiment. Ratio was estimated based on ion intensity.

Figure 4. (A) FTIR of HMW-DOM (red) and SPE DOM (blue); (B) A zoom-in of the carbonyl region showing a clear red-shift in HMW-DOM (red), but not in SPE DOM (blue), which may be a result of hydrogen bond connected to carbonyl groups (C) A schematic structure of HMW-DOM and its interaction with H_2O molecules is proposed. The proposed structure of HMW-DOM is built upon: (1) the majority of HMW-DOM can be explained by carbohydrate-like structure (*48*); (2) the relative abundance of different functional group should be consistent with the ^{13}C NMR results (*48*, *50*); (3) H_2O molecules are mainly bonded to the O in carbonyl group. The proposed structure has a formula of $C_{41}H_{79}N_3O_{40}$ and a molecular weight of 1253 (with H_2O included), with carbonyl carbon -**C**(O)- of 17%, anomeric carbon -O-**C**-O- of 15%, hydroxyl carbon -**C**-O- of 44%, amide carbon -**C**-N- of 7%, and alkyl C -**C**H/-**C**H_2/-**C**H_3 of 17%. A total of 7 H_2O molecules are bonded to the organic matter molecules, assisting the cross-linkage among carbohydrate-like structures. This is equivalent to a weight percentage of ca. 10% of H_2O, and 1 H_2O molecule for every 6 C.

Figure 5. Changes of DOC for two sets of incubation, with original HMW-DOM in red and H_2O-less DOM in blue.

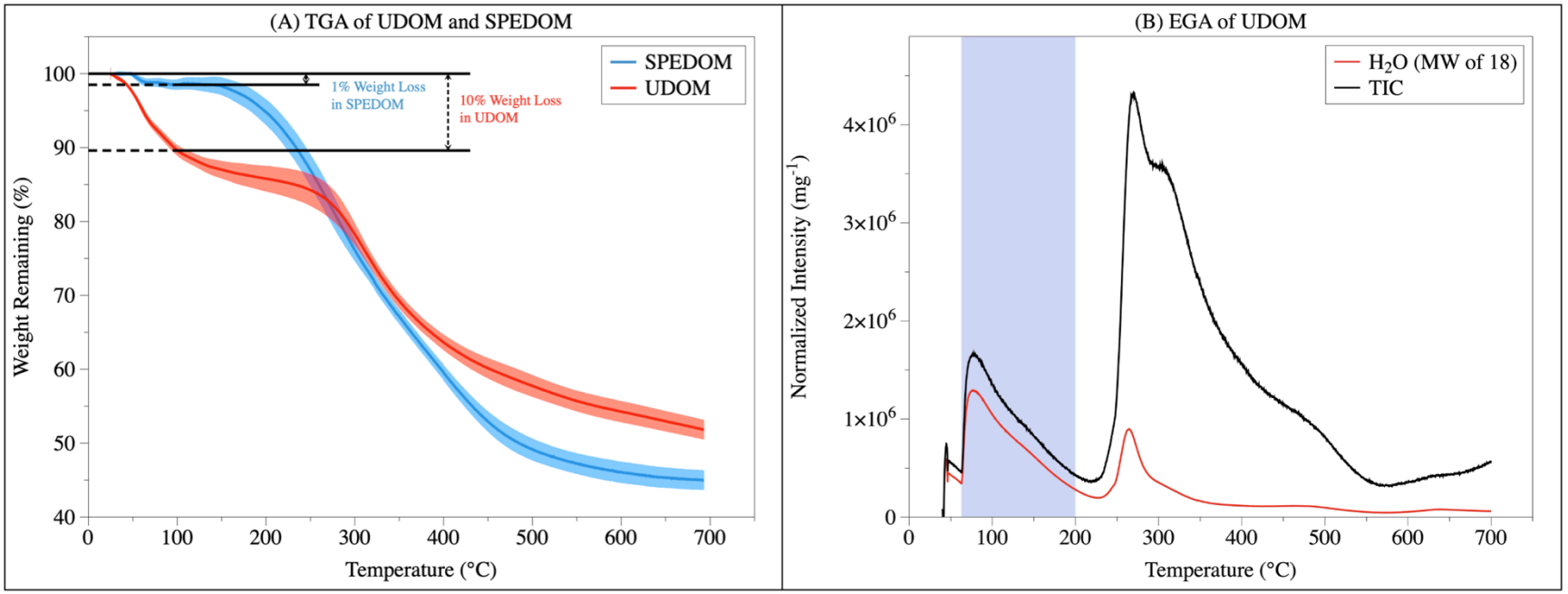

Figure 1. (A) Weight loss pattern of HMW DOM and SPE DOM from TGA; and (B) Chromatograms of volatile component from the EGA of HMW DOM. Shaded area in (B) indicates the region where most H_2O is detected.

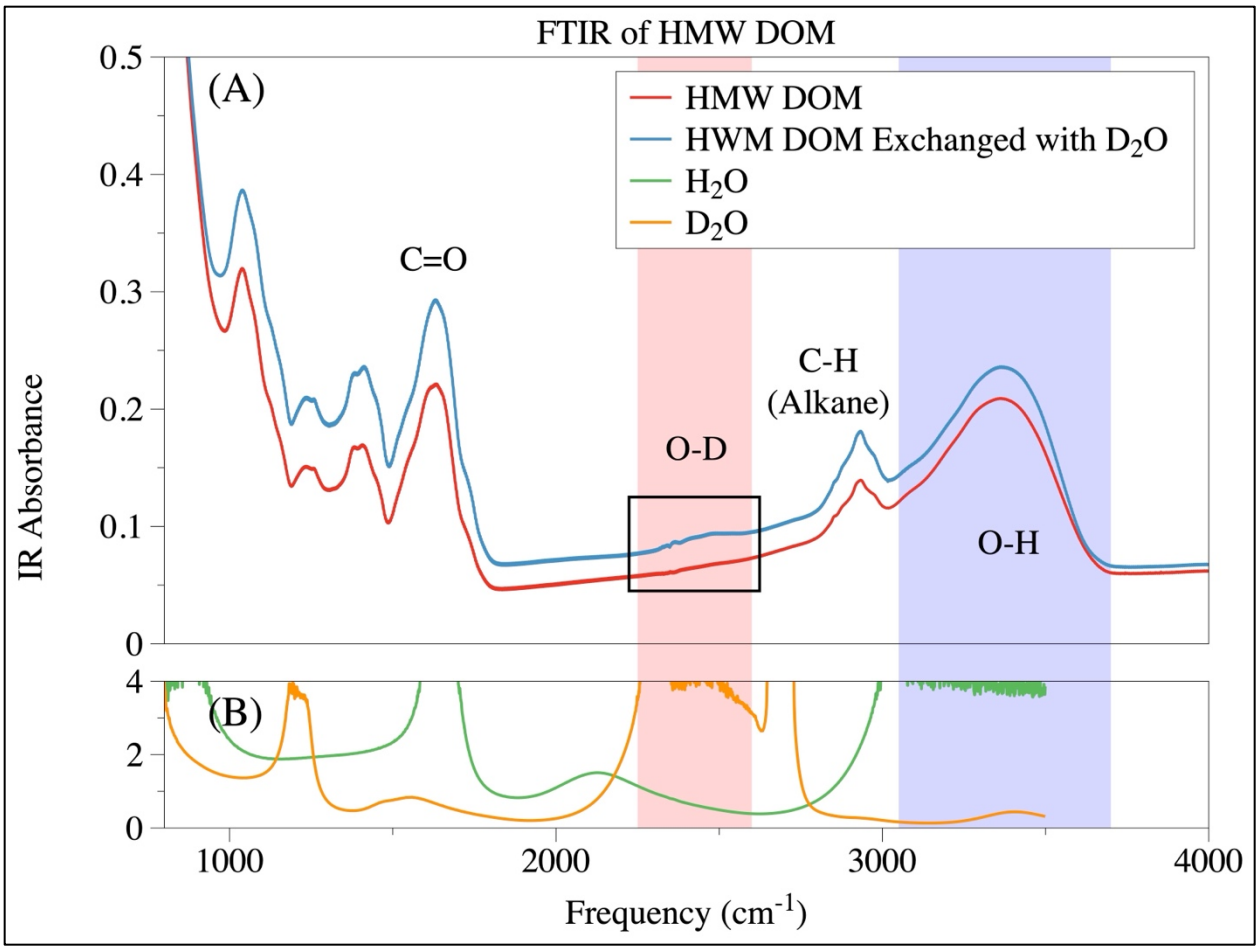

Figure 2. FT-IR spectra of (A) high molecular weight DOM (HMW DOM) obtained via ultrafiltration (red) and D_2O-exchanged HMW DOM (blue), with the O-D stretching absorption peaks highlighted; (B) spectra of the solvent D_2O (green) and H_2O (orange) for comparison.

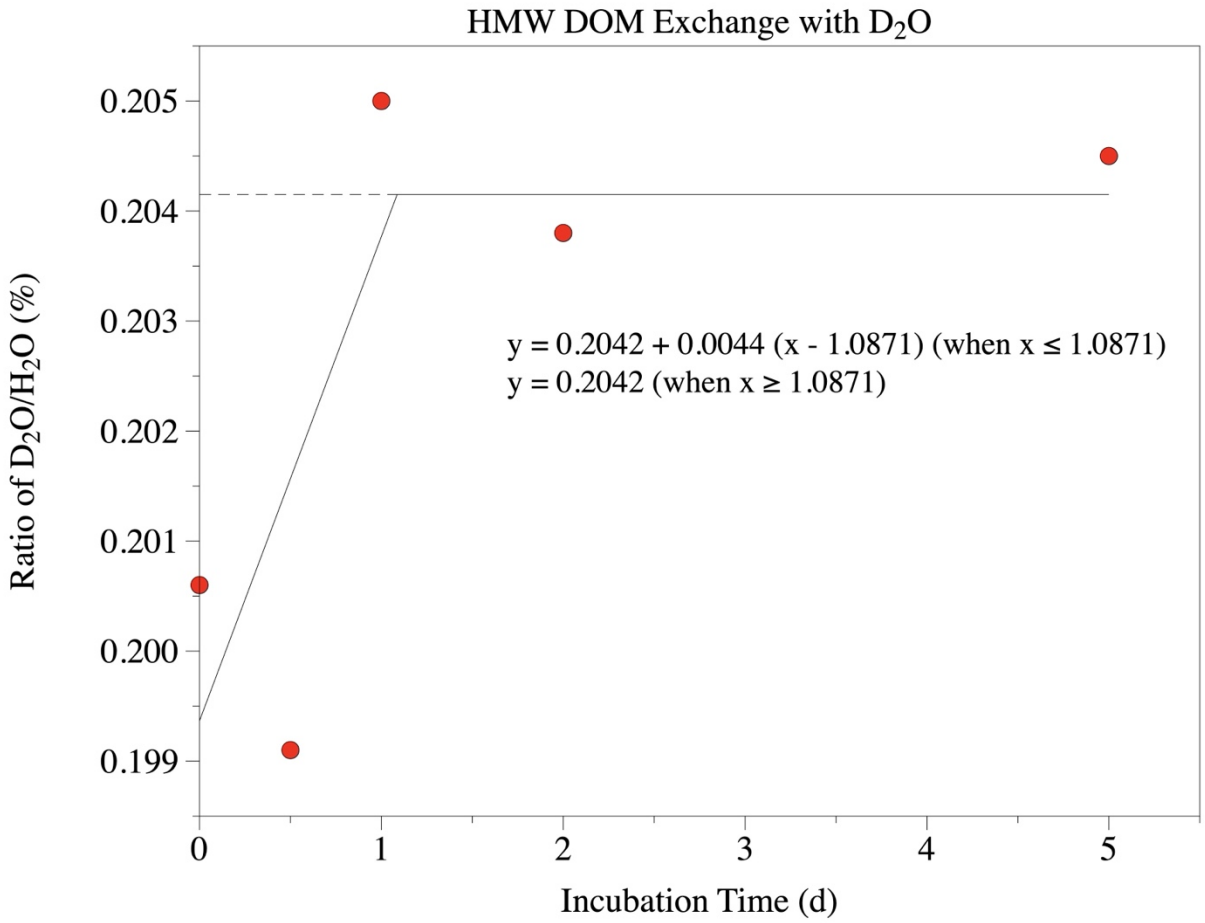

Figure 3. Change of D_2O/H_2O ratio during the D_2O exchange experiment. Ratio was estimated based on ion intensity.

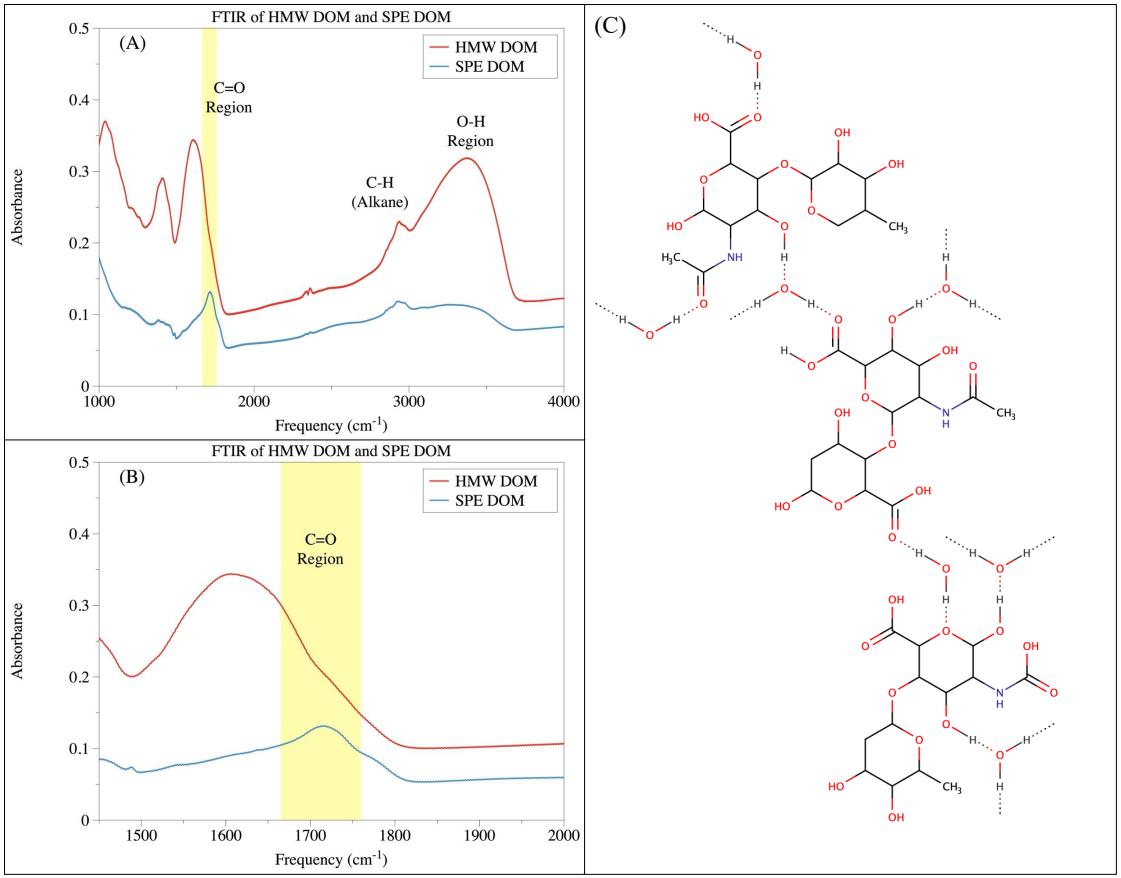

Figure 4. (A) FTIR of HMW DOM (red) and SPE DOM (blue); (B) A zoom-in of the carbonyl region showing a clear red-shift in HMW DOM (red), but not in SPE DOM (blue), which may be a result of hydrogen bond connected to carbonyl groups (C) A schematic structure of HMW DOM and its interaction with H_2O molecules is proposed. The proposed structure of HMW DOM is built upon: (1) the majority of HMW DOM can be explained by carbohydrate-like structure (42); (2) the relative abundance of different functional group should be consistent with the ^{13}C NMR results (42, 43); (3) H_2O molecules are mainly bonded to the O in carbonyl group. The proposed structure has a formula of $C_{41}H_{79}N_3O_{40}$ and a molecular weight of 1253 (with H_2O included), with carbonyl carbon -**C**(O)- of 17%, anomeric carbon -O-**C**-O- of 15%, hydroxyl carbon -**C**-O- of 44%, amide carbon -**C**-N- of 7%, and alkyl C -**C**H/-**C**H_2/-**C**H_3 of 17%. A total of 7 H_2O molecules are bonded to the organic matter molecules, assisting the cross-linkage among carbohydrate-like structures. This is equivalent to a weight percentage of ca. 10% of H_2O, and 1 H_2O molecule for every 6 C.

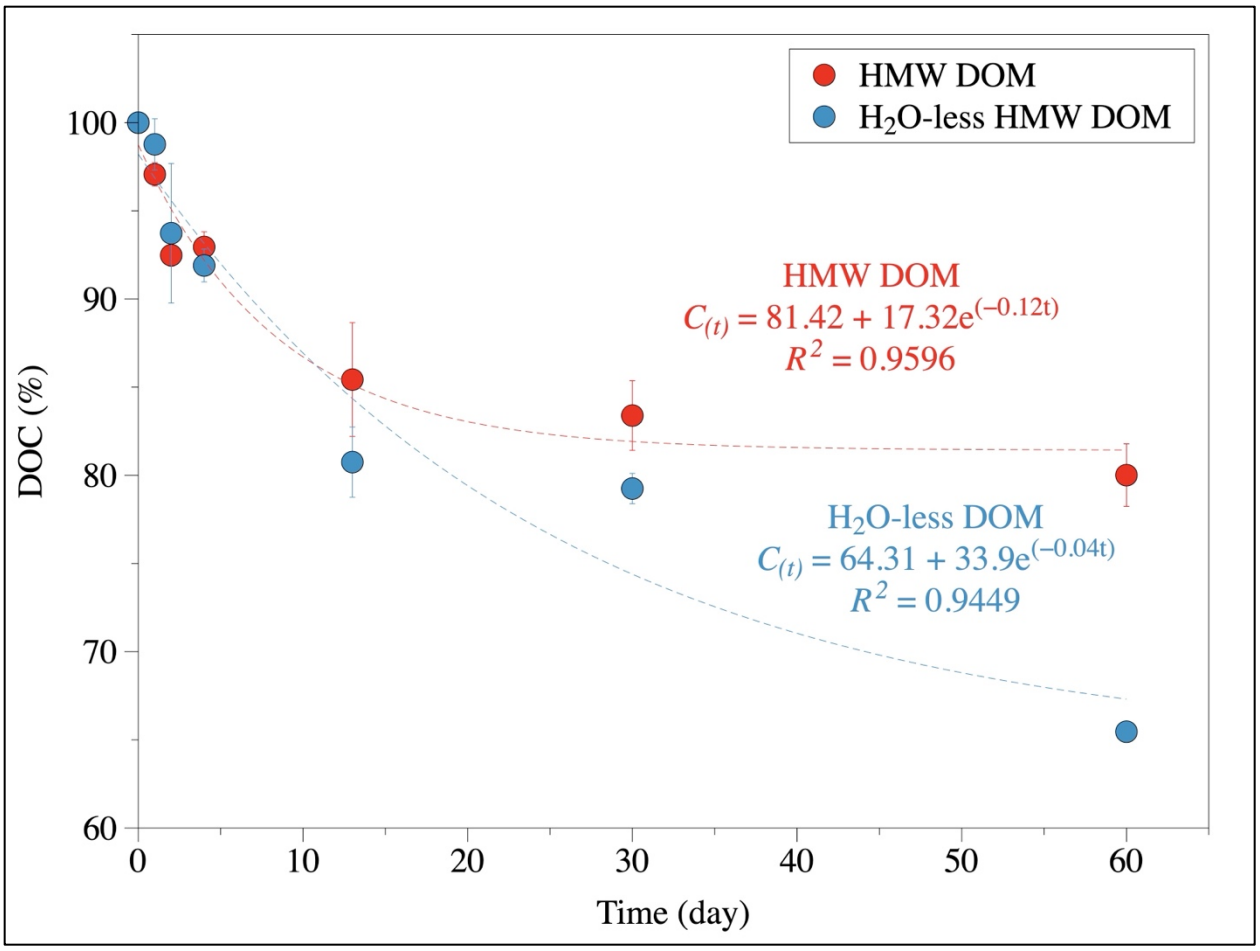

Figure 5. Changes of DOC for two sets of incubation, with original HMW DOM in red and H_2O-less DOM in blue.

Materials and methods

Sample collection. Sample collection was described in a previous study (*1*). Specifically, water samples were collected from south Texas rivers, including the Guadalupe River (GR; N 28.48°, W 96.86°), Mission River (MR; N 28.29°, W 97.28°), and Nueces River (NR; N 27.88°, W 97.63°), and one coastal site from a ship channel (SC; N 27.84°, W 97.05°, Port Aransas, Texas) that is connected to the open Gulf of Mexico (Figure S7). The three river water samples all had a salinity of < 1‰, representing freshwater DOM, whereas the coastal water sample had a salinity of ca. 30 ‰, representing marine DOM. An additional HMW-DOM sample was collected from the Gulf of Mexico (GOM; 28.51°N, 94.19°W) at 2 m depth with a salinity of 35.29‰ (*2*).

Water samples were collected with the pre-acid cleaned 10-L high-density polyethylene (HDPE) bottle or 20-L HDPE carboy and stored in a cooler with ice. Upon returning to lab within the same day, the samples were immediately filtered through in-series filter cartridges (Whatman™ Polycap HD 75 Capsule Filter, 5.0 µm, 2712 M; Whatman™ Polycap AS 75 Capsule filter, 0.2 µm, 2706 T) to remove suspended particles. The GOM water sample was directly pumped peristaltically through a 0.2 µm Nuclepore cartridge (Osmonics) to an ultrafiltration reservoir (*3*). Ultrafiltration of the 0.2 µm filtered water (without any pretreatment) was carried out with a spiral-wound Amicon S10N1 ultrafiltration cartridge (regenerated cellulose, Millipore), with a nominal molecule-weight cutoff of 1 kDa. After ultrafiltration, the retentate (reduced from 20 L to 0.5 L) was further diafiltered with 20 L of ultrapure water to remove residual low molecular weight DOM and salts (*4*). The purified HMW-DOM was then freeze-dried (*5*).

The SPE DOM was obtained from the same water sample following published protocols (*6*). Briefly, filtered (0.2 µm) and pre-acidified (pH of 2) water was passed through a methanol-conditioned PPL cartridge (Agilent). SPE DOM was eluted from the cartridge with LC/MS grade methanol. The solvent was then gently blown away with N_2 gas, and the SPE DOM was reconstituted in LC/MS grade water. Powder form of SPE DOM was obtained by freeze-drying the pre-frozen SPE DOM solution.

D_2O exchange experiment. To investigate the dynamics of bonded H_2O in HMW-DOM, a D_2O exchange experiment was conducted. Approximately 1 mg of HMW-DOM was dissolved in 2 mL of D_2O (99.9% atom% of D; 151882-25G, Sigma-Aldrich) in pre-combusted 20 mL scintillation bottle, and was placed in an oven maintained at a temperature of ca. 65 °C. At designated time points (0 hour, 12 hours, 24 hours, 48 hours, and 120 hours after the starting time point), one bottle was taken out and freeze dried for at least 48 hours to remove the excess D_2O. Freeze dried DOM samples were then analyzed using evolved gas analysis – gas chromatography mass spectrometry (EGA-GC/MS) to measure the amount of H_2O replaced by D_2O.

In-lab incubation of HMW-DOM and H_2O-less HMW-DOM. In-lab incubations were conducted to investigate the effect of bonded H_2O on the bioavailability of HMW-DOM. The H_2O-less HMW-DOM was obtained by pyrolyzing the original HMW-DOM in a thermogravimetric analyzer (Shimadzu TGA-50). HMW-DOM samples were heated under N_2 gas at a flow rate of 50

mL·min^{-1}, with temperature ramping from ca. 25 °C to 70 °C at a ramping rate of 20 °C·min^{-1}, and was held at 70 °C for 30 min. A pilot experiment confirmed that a 10% – 11% weight loss can be achieved as early as 8 min, and the weight of HMW-DOM remained constant under 70 °C for over 3 h (Figure S8). To test whether the low-temperature H_2O loss in HMW-DOM is reversible, a fraction of the pyrolyzed HMW-DOM was dissolved in LC/MS grade water, and dynamic light scattering (DLS) analysis was applied to monitor the change of solute size.

Unfiltered coastal seawater collected at the Ship Channel in Port Aransas, Texas, was used for incubation. The Ship Channel water has a salinity of 37 ‰, and a background DOC concentration of ca. 1 ppm. After transferring 150 mL of seawater into pre-combusted 250 mL amber glass bottle, the bottles were spiked with HMW-DOM or H_2O-less DOM to a final concentration of ca. 10 ppm, ten times higher than the ambient DOC. The setup is in triplicate (i.e., three HMW and three H_2O-less HMW). The headspace (ca. 120 mL) in the incubation bottle, together with the initial well-oxygenated water and the aerated sub-sampling, is enough to maintain oxic for the duration of the incubation. Incubation was carried out under room temperature (ca. 20 °C). At designated time points (day 0, 1, 2, 4, 13, 30, and 60), 10 mL subsamples were taken from each incubation bottle and filtered through a 0.2 μm cellulose acetate syringe filter. The filtrates were kept at -20 °C until further dissolved organic carbon (DOC) analysis with a TOC-L analyzer (Shimadzu). This left each incubation with over half of its initial volume by the end of the incubation, minimizing the potential effects caused by changing in water volume.

The incubation was also conducted with low-concentration HMW-DOM in artificial seawater, which was inoculated with unfiltered Ship Channel seawater at a ratio of 20:1 (*7*) (data in Figure S6). The concentrations of HMW-DOM and H_2O-less DOM were adjusted to ca. 3 ppm. Instead of taking subsamples from one large bottle, individual bottles were used for each time point. In addition to concentrations of DOC, levels of dissolved oxygen (DO) and microbial abundance at each sampling time were also monitored. The headspace of each incubation bottle was maintained at minimal level to exclude possible interference in DO measurement.

Specifically, at designated time points (day 0, 1, 6, 13, and 48), duplicate bottles of both HMW-DOM and H_2O-less DOM treatments were sacrificed, and measured for their DO with a Unisense micro-oxygen sensor. One-mL subsample from each incubation bottle was transferred into a 1.5 mL Eppendorf tube and preserved with 90 μL formaldehyde under 4 °C for microbial abundance analysis via a C6 flow cytometer (*8*, *9*). The rest samples were filtered through a 0.2 μm cellulose acetate syringe filter. The filtrates were kept at -20 °C until further dissolved organic carbon (DOC) analysis with a TOC-L analyzer (Shimadzu). Results of the artificial seawater incubations were included in the Supporting Information.

Thermogravimetric analysis (TGA) and evolved gas analysis (EGA). The thermogravimetric analysis (TGA) was carried out with a thermogravimetric analyzer (Shimadzu TGA-50). HMW-DOM samples, in ca. 2 mg, were pyrolyzed under N_2 gas at a flow rate of 50 mL·min^{-1}, with temperature ramping from room temperature (ca. 25 °C) to 700 °C at a ramping

rate of 20 °C·min^{-1}. The weight of the remaining sample was measured every second, and the thermograms were generated using the LabSolution software (LabSolutions TA: Acquisition Version 1.00 SP1).

The evolved gas analysis (EGA) was conducted with a pyrolyzer (EGA/PY-3030D, Frontier 96 Laboratories Ltd.) coupled with a gas chromatography-mass spectrometer (GC-MS; Shimadzu GCMS-TQ8040). The pyrolysis was conducted under helium (He), and the pyrolyzer was set to ramp from 50 °C to 650 °C at a constant heating rate of 20 °C·min^{-1}, consistent with the TGA settings. An Ultra ALLOY EGA tube (ID: 0.15 mm, OD: 0.47 mm, length: 2.5 m; Frontier) was used and the GC oven was held at 300 °C. The ionization is electron impact ionization (EI). The mass spectrometer was programed to detect ions with a molecular weight range of 10 – 600 Da. Additionally, a set of specific molecular weights, including 18, 20, 32, and 44, were also monitored under single ion monitoring mode (SIM). The acquired chromatograms and spectra data were processed with the LabSolution software (GCMS solution, Version 4.45 SP1, Shimadzu).

FTIR analysis (need input from Dr. Baiz's group). FTIR spectra were recorded using a Bruker Vertex 70 spectrometer. To minimize interference from atmospheric water vapor absorption, both the spectrometer and sample chamber were purged with dry air throughout the measurements. Solid samples, of DOM before and after D_2O exchange, were placed between two CaF_2 windows with a 25 μm Teflon spacer to maintain a consistent path length. All samples were kept at room temperature. The spectra were collected in the mid-infrared region (4000–400 cm^{-1}) at a resolution of 4 cm^{-1}, with 64 scans averaged per spectrum. A background scan was measured before each sample measurement. The spectra are not baseline corrected, and the baselines are not zero due to scatter of the IR light by the solid DOM samples.

2D IR Spectroscopy. Ultrafast 2D IR spectra were measured using a custom-built pulse-shaper-based spectrometer, as previously described (*10*). In summary, 2D IR measurements involved excitation (pump) and detection (probe) pulses, both tuned to the carbonyl stretching region. Pump and probe pulses were centered around 1700 cm^{-1} with a FWHM of ~300 cm^{-1}. Coherence times (t_1) were scanned up to 3 ps in 20 fs steps using a rotating frame. Spectra were measured at a waiting time of 150 fs and 500 fs. The probe pulse was dispersed into a 128×128-pixel MCT array to generate the detection axis. The polarization was set to perpendicular to reduce scatter from the sample. The same samples used for FTIR, described above, were measured in the 2D IR spectrometer. The resulting 2D IR spectra display the characteristic positive-negative peak doublet, representing the ground-state bleach (red contours along the diagonal) and excited-state absorption (blue contours below the diagonal), as illustrated in Figure S4.

Data presentation. Marvin is used for drawing the schematic model of the HMW-DOM (Marvin 17.21.0, Chemaxon; https://www.chemaxon.com). The map for sampling locations is created with QGIS (3.28.9). The rest figures are created with DataGraph (DataGraph 5.3).

Supporting Figures

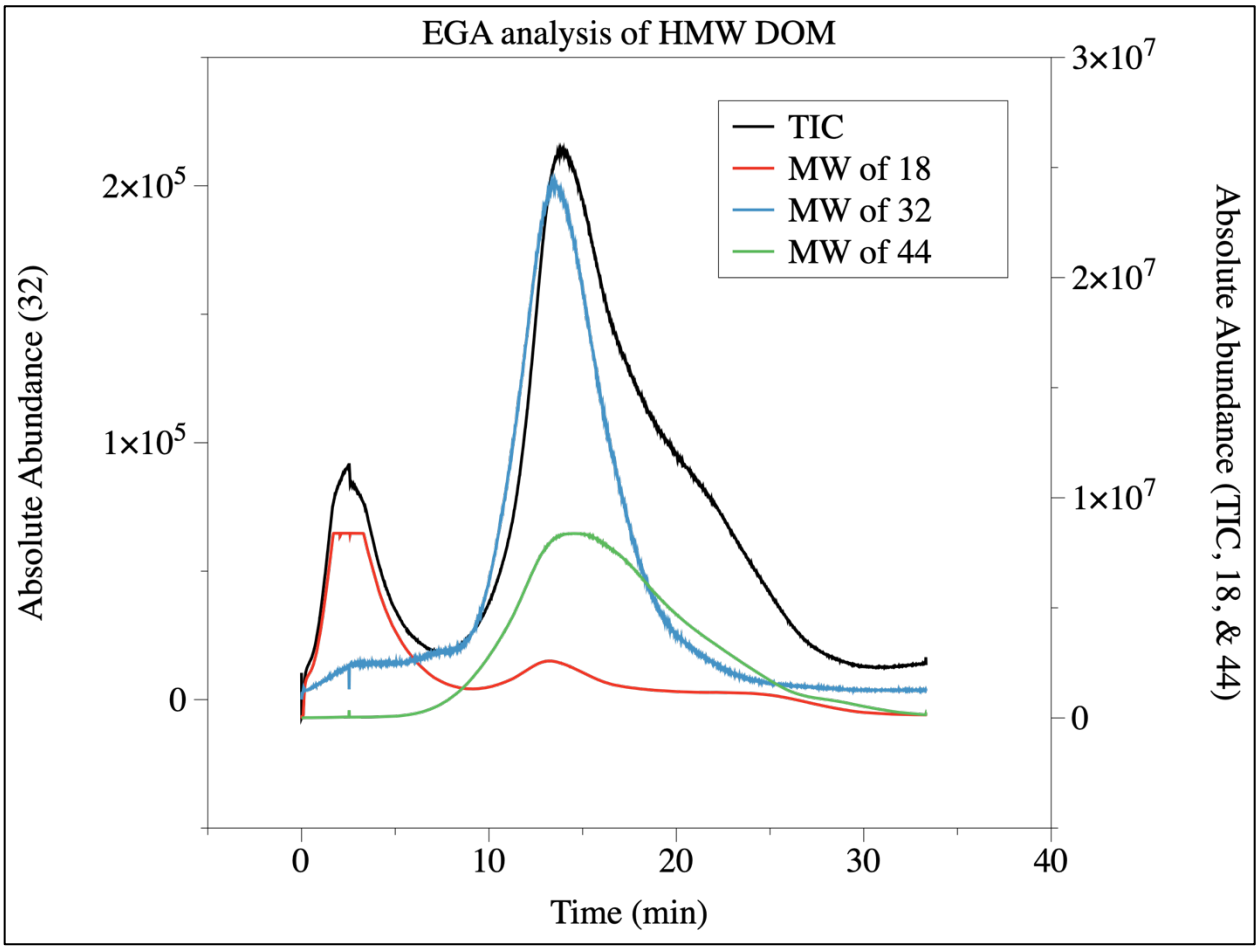

Figure S1. The evolved gas analysis (EGA) chromatograms of HMW DOM, showing the total ion chromatogram (TIC; black), compound with molecular weight (MW) of 18 Da (red), 32 Da (blue), and 44 Da (green). Electron ionization (EI) uses energetic electrons to produce ions from gas or solid phase atoms or molecules. Therefore, the detected *m/z* can be considered as the MW of the volatile compound. The MW of 18, 32, and 44 represent H_2O, CH_3OH, and CO_2, respectively.

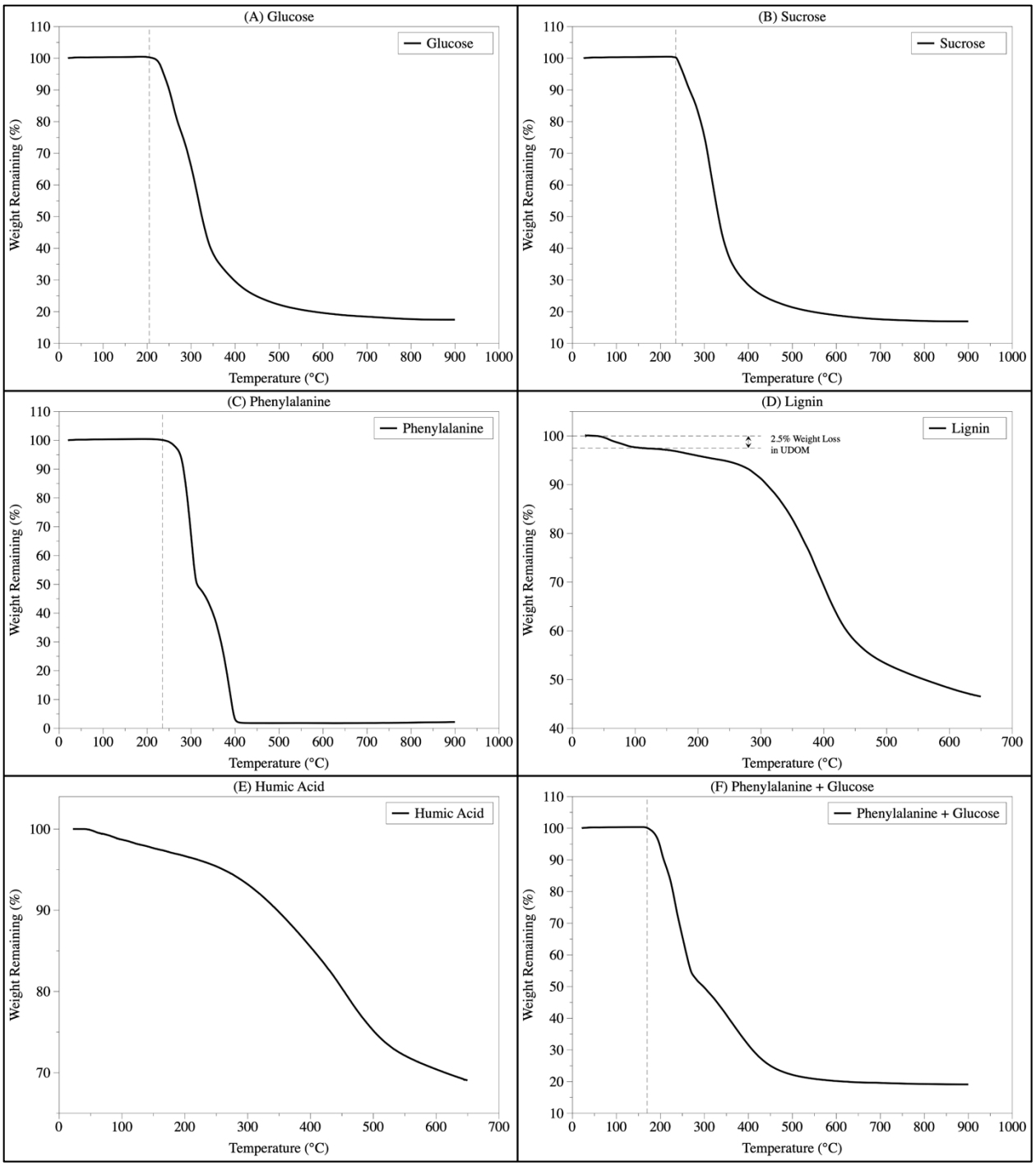

Figure S2. TGA chromatograms of (A) glucose, (B) sucrose, (C) phenylalanine, (D) lignin (E) humic acid, and (F) mixture (1:1 by weight) of phenylalanine and glucose. For the pure biomolecules (i.e., glucose, sucrose, and phenylalanine), no weight loss was observed until the temperature reached over 200 °C. Natural mixtures (i.e., lignin and humic acid), on the other hand, resembled the pattern seen in SPE DOM.

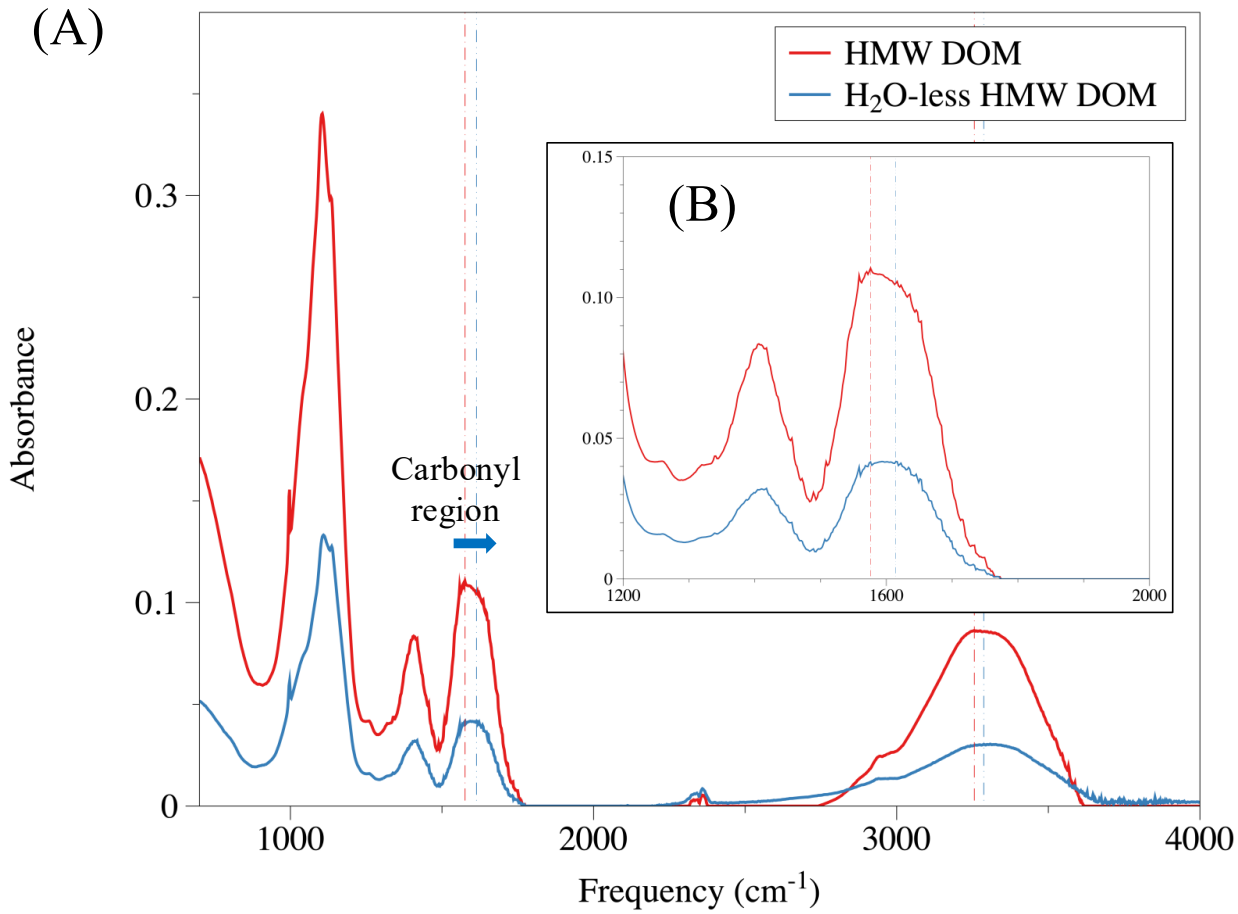

Figure S3. Comparison of the FTIR spectra of HMW-DOM (red) and H_2O-less HMW-DOM (blue) shows a slight blueshift of carbonyl region when the bonded-H_2O is removed through low temperature pyrolysis (A). The carbonyl region is enlarged, and the shift is more obvious, from 1576 cm^{-1} in HMW-DOM to 1614 cm^{-1} in H_2O-less HMW-DOM (B).

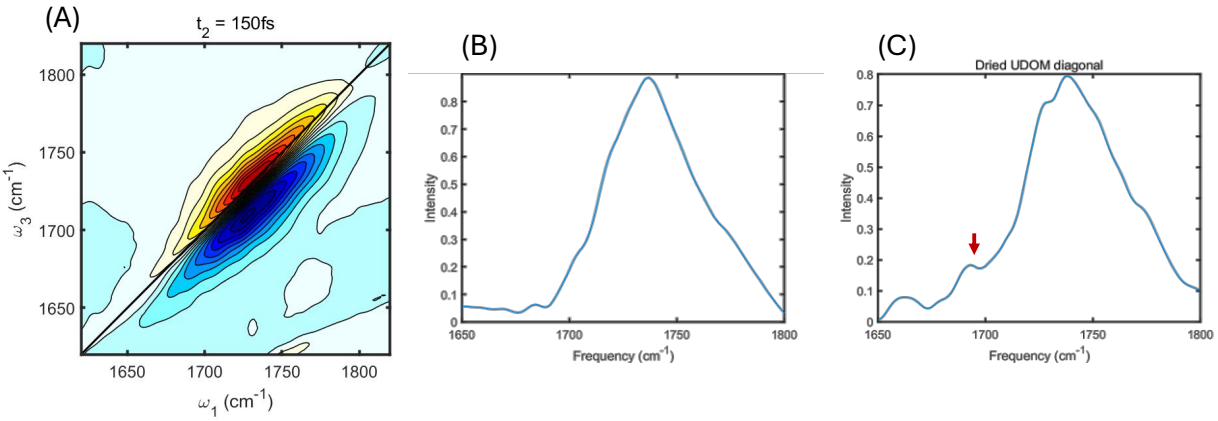

Figure S4. (A) 2D IR spectra of HMW DOM at a 150 fs delay. Diagonal slices of the 2D spectra at 150 fs (B) and 500 fs (C), showing fundamental vibrational frequencies of the carbonyl group in the DOM samples. The diagonal slices of the 2D IR spectra reveal the fundamental vibrational frequencies of the carbonyl groups in the HMW DOM. The broadening observed along the diagonal indicates a heterogeneous system, with multiple environments contributing to the spectral features. The lower wavenumber carbonyl peak, associated with hydrogen-bonded carbonyl groups, weakens at longer delay times (indicated by the arrow), which can be attributed to vibrational relaxation.

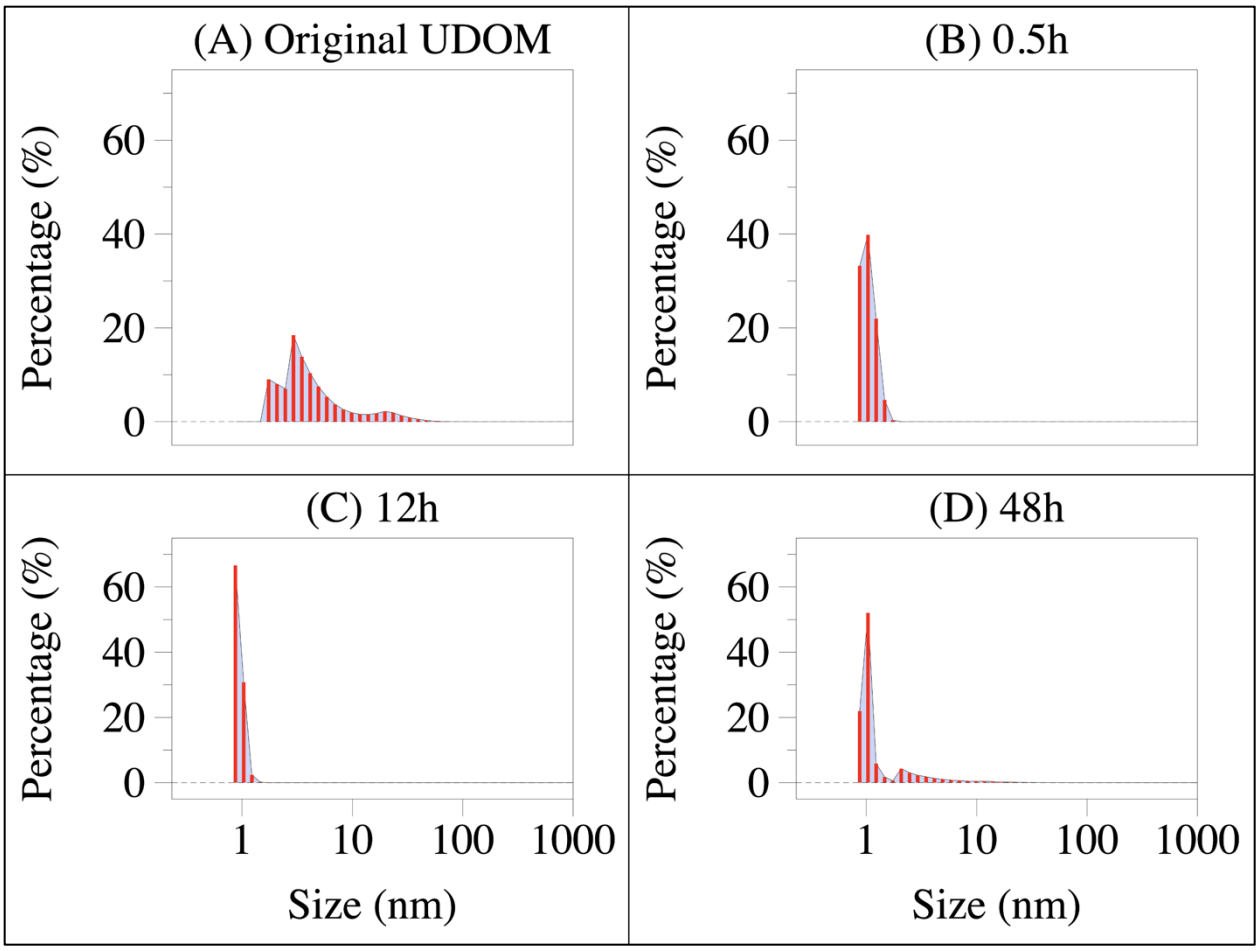

Figure S5. DLS showing the solute size of H_2O-loss DOM. HMW DOM was pyrolyzed at a relatively low temperature (70 °C) and subsequently re-dissolved it in LC/MS grade water. Dynamic light scattering (DLS) analysis revealed a pronounced reduction in solute size after the low-temperature pyrolysis, transitioning from a wide size distribution spanning 1 nm to nearly 100 nm (average size of ca. 10 nm) to a much narrower distribution centered around 1 nm. Notably, no reconstitution of H_2O-loss DOM occurred even after 48 hours.

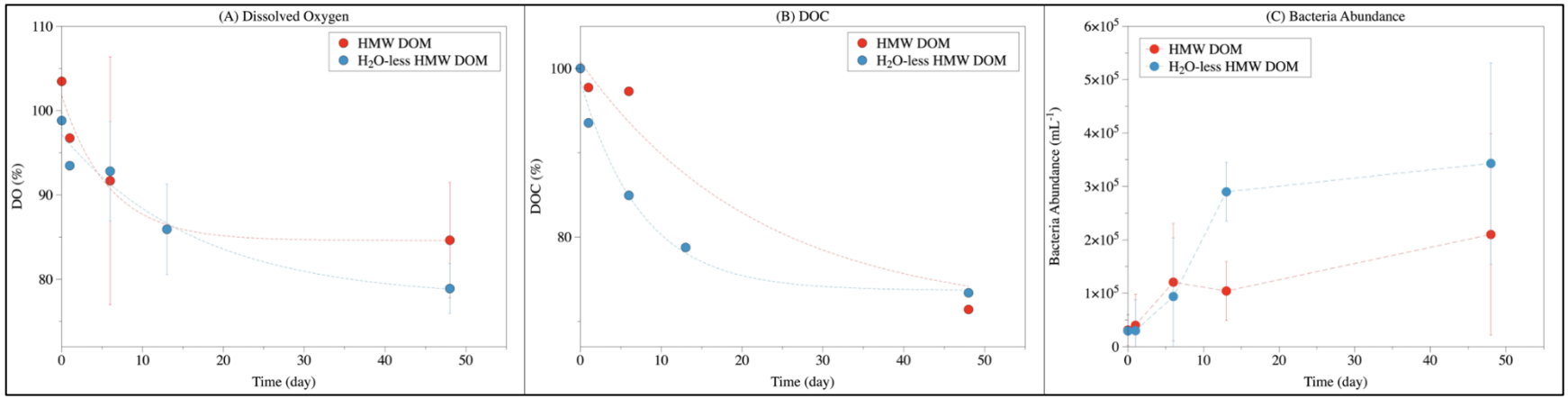

Figure S6. The change of (A) DO, (B) DOC, and (C) microbial abundance in the repeated incubation (inoculation to the artificial seawater). A higher consumption of DO and a higher bacteria abundance was observed for the H_2O-less HMW DOM, supporting the idea that the removal of bonded H_2O increases the bioavailability of HMW DOM, even though the DOC concentrations were quite similar by the end of incubations between two treatments. The rather similar DOC concentrations may be due to the fact that the DOC concentration is approaching the detection limit of the instrument.

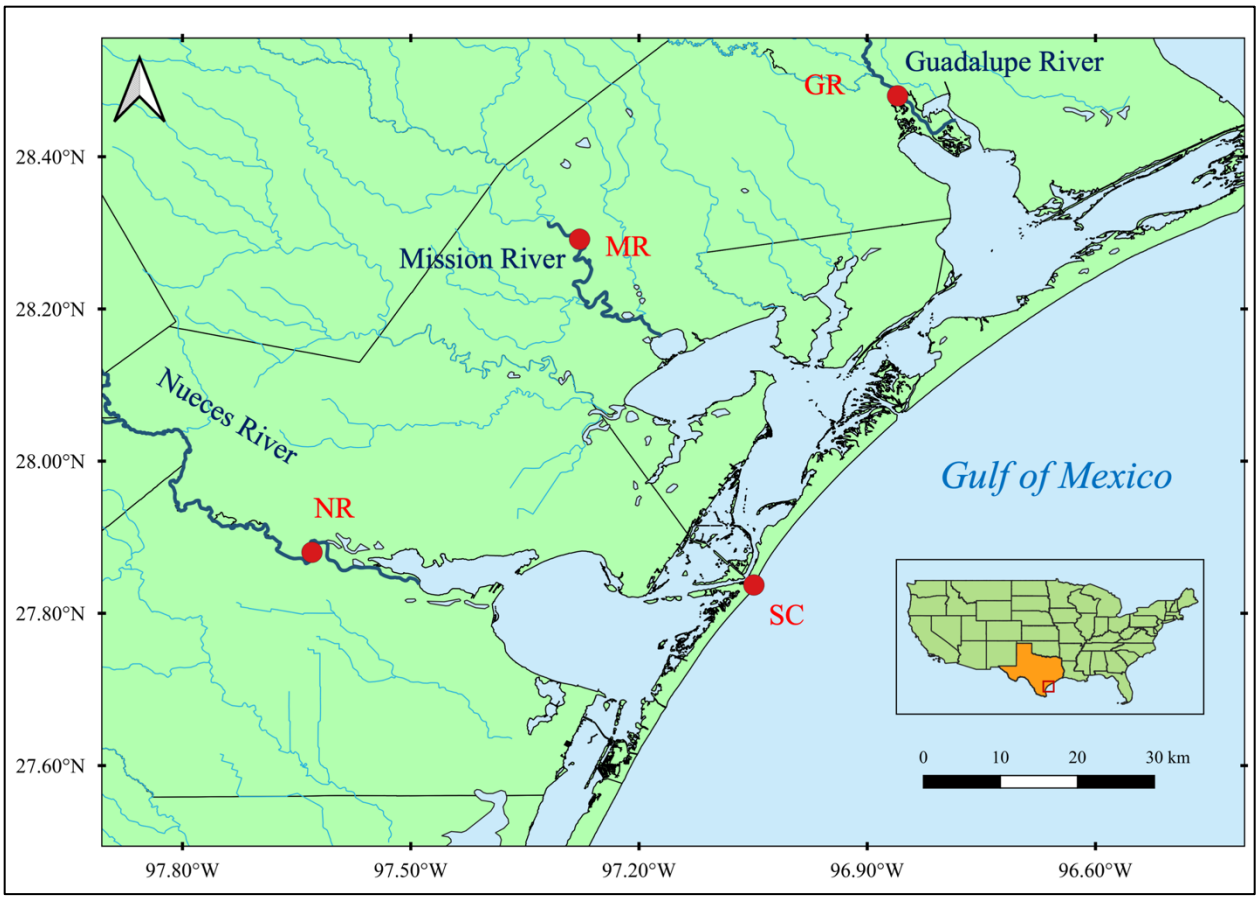

Figure S7. Sampling map. Water samples were collected from Guadalupe River (GR; N 28.48°, W 96.86°), Mission River (MR; N 28.29°, W 97.28°), and Nueces River (NR; N 27.88°, W 97.63°), and one coastal site from a ship channel (SC; N 27.84°, W 97.05°, Port Aransas, Texas. The three river water samples all had a salinity of < 1‰, representing freshwater DOM, whereas the coastal water sample had a salinity of ca. 30 ‰, representing marine DOM. An additional HMW DOM sample was collected from the Gulf of Mexico (GOM; 28.51°N, 94.19°W; not shown in the map) at 2 m depth with a salinity of ca. 35‰

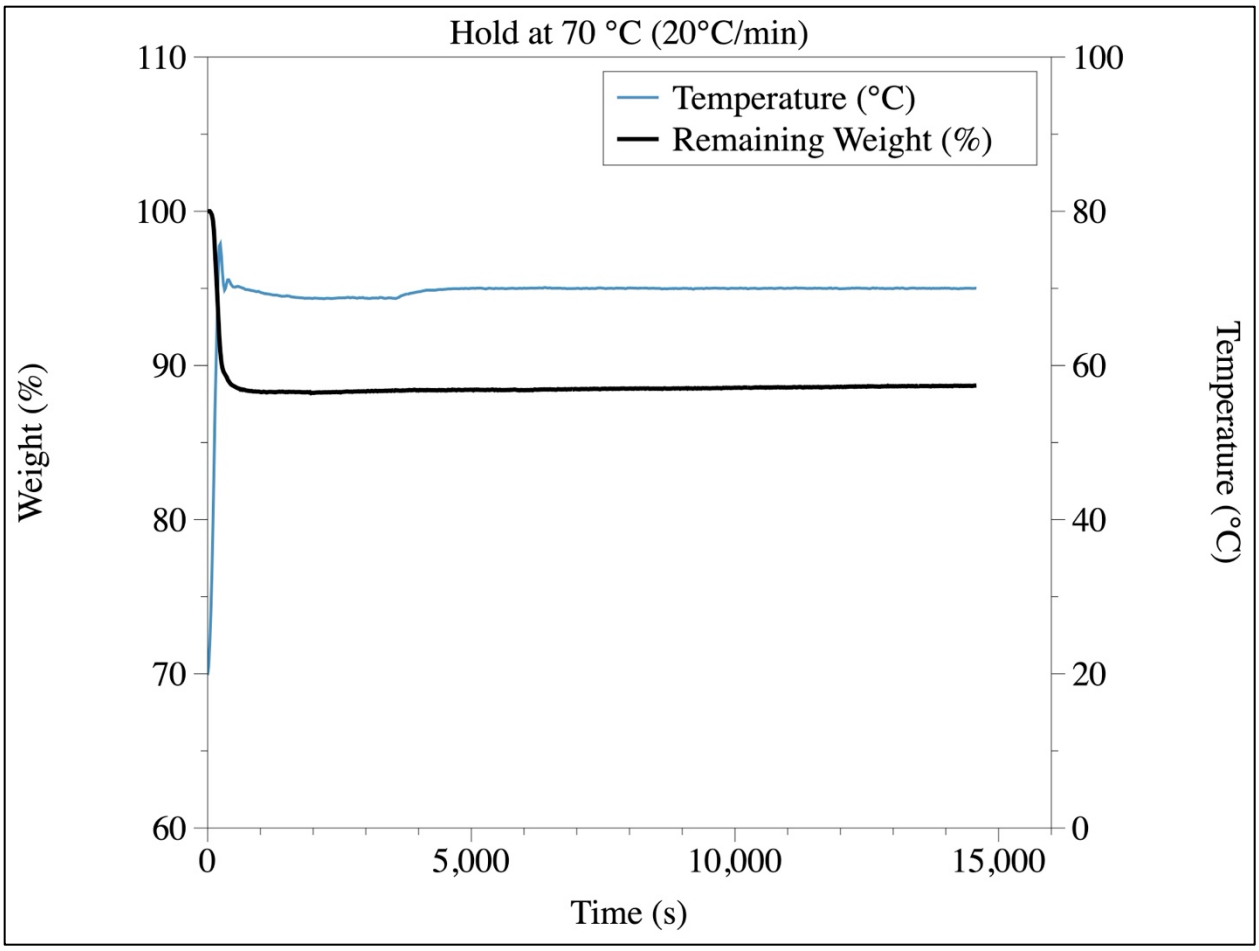

Figure S8. TGA of HMW DOM. Ramping rate: 20 ℃/min; hold temperature: 70 ℃; hold time: 4 hours. A rapid weight loss of ca. 11% was achieved within the first 8 – 10 minutes of the pyrolysis process. However, the weight of HMW DOM remained constant at 70 ℃ for the nearly 3 hours.

References

1. K. Lu, J. Xue, L. Guo, Z. Liu, The bio- and thermal lability of dissolved organic matter as revealed by high-resolution mass spectrometry and thermal chemical analyses. *Mar. Chem.*, 104184 (2022).

2. C.-C. Hung, L. Guo, P. H. Santschi, N. Alvarado-Quiroz, J. M. Haye, Distributions of carbohydrate species in the Gulf of Mexico. *Mar. Chem.* **81**, 119–135 (2003).

3. L. Guo, P. H. Santschi, L. A. Cifuentes, S. E. Trumbore, J. Southon, Cycling of high-molecular-weight dissolved organic matter in the Middle Atlantic Bight as revealed by carbon isotopic (13C and 14C) signatures. *Limnol. Oceanogr.* **41**, 1242–1252 (1996).

4. L. Guo, P. H. Santschi, A critical evaluation of the cross-flow ultrafiltration technique for sampling colloidal organic carbon in seawater. *Mar. Chem.* **55**, 113–127 (1996).

5. H. Lin, H. Xu, Y. Cai, C. Belzile, R. W. Macdonald, L. Guo, Dynamic changes in size-fractionated dissolved organic matter composition in a seasonally ice-covered Arctic River. *Limnol. Oceanogr.* **66**, 3085–3099 (2021).

6. T. Dittmar, B. Koch, N. Hertkorn, G. Kattner, A simple and efficient method for the solid-phase extraction of dissolved organic matter (SPE-DOM) from seawater. *Limnol Ocean. Methods* **6**, 230–235 (2008).

7. K. Wu, K. Lu, M. Dai, Z. Liu, The bioavailability of riverine dissolved organic matter in coastal marine waters of southern Texas. *Estuar. Coast. Shelf Sci.* **231**, 106477 (2019).

8. Z. Liu, S. Liu, High phosphate concentrations accelerate bacterial peptide decomposition in hypoxic bottom waters of the northern Gulf of Mexico. *Environ. Sci. Technol.* **50**, 676–684 (2016).

9. K. Lu, Z. Liu, R. Dai, W. S. Gardner, Urea dynamics during Lake Taihu cyanobacterial blooms in China. *Harmful Algae* **84**, 233–243 (2019).

10. S. C. Edington, A. Gonzalez, T. R. Middendorf, D. B. Halling, R. W. Aldrich, C. R. Baiz, Coordination to lanthanide ions distorts binding site conformation in calmodulin. *Proc. Natl. Acad. Sci.* **115**, E3126–E3134 (2018).